Doppler radar analysis of a tornadic miniature supercell during the Landfall of Typhoon Mujigae (2015) in South China

Kun Zhao*[#], Mingjun Wang[#] ,Ming Xue[#,%], Peiling Fu[#],
Zhonglin Yang[#] , Xiaomin Chen[#] and Yi Zhang[#]
[#]Key Lab of Mesoscale Severe Weather/Ministry of Education of China,
and School of Atmospheric Sciences, Nanjing University, Nanjing, China
[%]Center for Analysis and Prediction of Storms and School of Meteorology, University of Oklahoma, Norman Oklahoma 73072, USA

Wen-Chau Lee
Earth Observing Laboratory, National Center for Atmospheric Research[1]
Boulder, Colorado

Fuqing Zhang
Department of Meteorology and Atmospheric Science, and Center for Advanced Data Assimilation and Predictability Techniques, the Pennsylvania State University,
University Park, Pennsylvania

Qing Lin and Zhaohui Li
Guangdong Meteorological Observatory, and Foshan tornado research Center,
Guangdong Meteorological Service, Guangzhou, China

28 June 2016
Submitted to Bulletin of the American Meteorological Society
Revised October 31, 2016

*Corresponding author address:
Dr. Kun Zhao
Key Laboratory of Mesoscale Severe Weather/MOE,
School of Atmospheric Sciences, Nanjing University,
163 Xianlin Road, Nanjing 210023, China
zhaokun@nju.edu.cn

[1] National Center for Atmospheric Research is sponsored by the National Science Foundation.

Abstract

On 4 October 2015, a miniature supercell in the outer rainband of landfalling Typhoon Mujigae produced a violent tornado in Guangdong Province of South China, leading to 4 deaths and up to 80 injuries. A detailed damage survey shows that the tornado is rated at least a category 3 on the enhanced Fujita scale (EF3), which is by far the strongest typhoon rainband tornado ever documented in China. This study, for the first time, documents the structure and evolution of the tornadic miniature supercell and the environmental conditions with observations from coastal Doppler radars and a nearby sounding.

Radar analysis indicates that this tornadic, miniature supercell exhibited characteristics similar to those found in landfalling hurricanes in the US, whose signatures include a hook echo, several low-level inflow notches, an echo top below 10 km, a small and shallow mesocyclone, and a long lifespan (~3 h). The environmental conditions characterized by the nearby sounding consisted of moderate CAPE (~1284 J kg^{-1}), large veering low-level vertical wind shear, and large cell-relative helicity that are favorable for producing miniature supercells. The mesocyclone, with its maximum intensity at ~2 km above ground level (AGL), formed an hour before the tornadogenesis. A tornado vortex signature (TVS) was first identified between 1 and 3 km AGL, when its parent mesocyclone reached its peak intensity of 30 m s^{-1}. The TVS was located between the updraft and forward-flank downdraft, near the center of the mesocyclone. Dual-Doppler wind analysis reveals that tilting of low-level vorticity into the vertical direction and subsequent stretching by a strong updraft were the main contributors to the mesocyclone intensification.

1. Introduction

Tropical cyclone (TC)-spawned tornadoes often occur in the outer rainbands located in the right-front or the northeast quadrant relative to the TC track within a 200-400 km annulus (Edwards 2012; Schultz and Cecil 2009). These tornadoes often reside in miniature supercells in an environment characterized by high low-level moisture content, moderate convective available potential energy (CAPE), and enhanced low-level shear due to increased surface friction from water to land as well as boundary layer convergence (Green et al. 2011). Generally, these miniature supercells exhibit hook echo/appendage and tornado vortex signature (TVS) in Doppler radar observations (Mccaul 1987; Mccaul et al. 2004). Rare dual-Doppler observations (e.g, Lee et al. 2008; Eastin et al. 2009) had provided snapshots of the kinematic and dynamic structures of miniature supercells in the United States (US) in the past. In Asia, TC-spawned tornadoes and their parent miniature supercells have been observed by single Doppler radars in Japan and China (e.g. Saito et al. 1992; Suzuki et al. 2000; Zheng et al. 2015), revealing similar radar signatures as in their US counterparts. In China, typhoon-rainband-spawned tornadoes occur about once per year (Zheng et al. 2015). Nevertheless, the evolution, three-dimensional structures and other dynamic characteristics of miniature supercells in Asia have yet to be documented through dual-Doppler wind analysis. For reference, in China, the average number of tornadoes per year over the past half a century is fewer than 100, and the total number of the EF3 (enhanced Fujita scale) intensity or higher tornadoes is 20 (Xue et al. 2016; Fan and Yu 2015).

In the afternoon of October 4, 2015, two tornadoes were produced within the rainbands of typhoon Mujigae (2015) in Guangdong Province. Typhoon Mujigae was categorized as a super typhoon [those with peak wind speed of 51 m s^{-1} or greater Yu et al. (2013)] by the Chinese Meteorological Administration (CMA) near the time of landfall in Guangdong Province at 1400 LST on 4 October 2015, with the maximum sustained surface winds of 52 m s^{-1} and the minimum mean sea-level pressure (MSLP) of 935 hPa (Fig. 1). This destructive typhoon resulted in 19 deaths and 24 billion RMB losses in China, and as a result its name has been retired by the World Meteorological Organization. After its landfall, Mujigae produced two confirmed tornados and one waterspout within three separate miniature supercells in two outermost rainbands (Fig. 1). The strongest tornado, spawned in the third rainband from the center, was located ~350 km northeast of the Mujigae's center and was rated EF3 (enhanced Fujita scale), causing 4 deaths, 80 injuries, and about 2 million RMB damages in the city of Foshang. These rainbands were accompanied by active lightning over the ocean but lightning activities diminished over land. There were eight cloud-to-cloud lightning reports associated with this tornadic mini-supercell, all to the right of the supercell, but no hail was reported. Because of the relative rarity of tornadoes in China, tornado forecasting and warning operations had not been part of the routine operations of CMA. After a number of recent significant tornadoes, CMA is, however, starting experimental tornado forecasting and warning operations in several provinces including the Guangdong Province (Xue et al. 2016).

Doppler radar data were collected from Guangzhou (GZ) and Shenzhen (SZ) over a 90-min period while the target miniature supercell was located in the western dual-Doppler lobe (Fig. 1). The purpose of this study is to document, for the first time, the time evolution of the strongest TC-spawned tornado ever observed by modern instruments in China, as well as the evolution and structure of the parent mesocyclone and miniature supercell. The paper also compares and contracts the characteristics of the parent mesocyclone of this TC-spawned tornado with its US counterparts using the Doppler radar data from the closer GZ radar while coarser-resolution dual-Doppler wind analyses are used to examine the intensification mechanisms of the mesocyclone via vorticity budget analysis.

2. Environmental conditions and damage survey

The environmental conditions of the TC miniature supercell are shown by a rawinsonde profile (Fig. 3), released outside the distant rainband from the Hong Kong International Airport at 0600 UTC (1400 LST, all times hereafter are LST), an hour before the miniature supercell became tornadic. The key buoyancy and shear parameters (Fig. 3) meet the "high threat" category of a TC-spawned tornado in the US (Mccaul 1991; Schneider and Sharp 2007)

Joint damage surveys were conducted jointly by CMA, Nanjing University and Peking University. Aerial photography along the damage path from location LD to YB

(Fig. 2) was taken by an unmanned aerial vehicle operated by the Foshan Meteorological Bureau during 8 – 10 October. Ground damage surveys were also conducted to mark the directions of fallen walls, trees, and power poles. Considering the differences in building codes between China and the United States, as well as the soil properties affecting tree mortalities, the wind speed estimations of the matched degree of damage (DOD) were assigned the expected values (EXP in McDonald and Mehta 2006) for all of the damage indicators (DIs) (Meng and Yao 2014). Visual evidences (e.g., photographs and videos) of the tornado were also collected from a variety of sources (e.g., from news websites and a variety of online social media, etc.), which provided direct evidence of the tornado and the severity of its damages. The most severe damages were rated EF-3 as recommended by the Wind Science and Energy Center (McDonald and Mehta 2006).

The tornado's damage track was about 30 km long (Fig. 2c, white line). The wind damage first appeared to the southeast of location LD, but without clear tornado damage patterns. The tornado's parent supercell moved north-northwestward with a mean speed of ~21 m s^{-1}. At location LY, a funnel cloud was captured by a cellphone camera ~153124 (Fig. 2a) by Mr. S. Huang (available on youku.com), suggesting that the tornado touched down between LD and LY. Ten seconds later at 153134, two funnels are apparent (Fig. 2e). Several factory buildings were completely demolished by the tornado between LD and LY, with a damage swath ~150 m (Fig. 2b). The DI of this metal building with DOD 8 was rated EF3. The tornado then hit location SB ~1534 and damaged a larger area of metal buildings (rated EF3, not shown). A concrete electrical transmission line pole was snapped (Fig. 3d) north of location MD (rated EF3). The tornado kept intensifying and broadening, and reached its widest damage path ~500 m at location YB with the same DOD as those in LY and SB (figure not shown). Later, trees up to 20 cm in diameter were uprooted at location FS ~1543 (rated EF1, not shown).

3. Radar signatures of the miniature supercell, mesocyclone and tornado

3.1 Miniature supercell and mesocyclone

The damage track matched well with the "hook echo" radar reflectivity signature and the accompanied Doppler velocity dipole where V_{max} and V_{min} are the outbound and inbound Doppler velocity maxima (Fig. 4). A mesocyclone usually has a diameter between 2 to 10 km and a vertical vorticity on the order of 0.01 s^{-1} or greater (Glickman 2000). Figure 5 illustrates the characteristics of the mesocyclone from the axisymmetric rotational velocity, $V_{rot} = (V_{max} - V_{min})/2$, and the mesocyclone diameter, D, defined as the distance between V_{max} and V_{min} (Stumpf et al. 1998; Lee and White 1998), and azimuthal shear (one half of the vorticity), $(V_{max} - V_{min})/D$. The cyclonic vortex associated with the tornado-producing miniature supercell (Fig. 5) already met the criteria of a mesocyclone (Andra 1997; Lee and White 1998) with a vorticity exceeding 10^{-2} s^{-1} at 1430 and ~3 km AGL. The mesocyclone rapidly intensified below the 3 km altitude with a V_{rot} of up to 30 m s^{-1} at 1530. It can be categorized as strong mesocyclone according to the mesocyclone strength nomogram (Andra 1997). Associated with the strengthening mesocyclone, it contracted in diameter from ~6 km to less than 3 km at 1530 when the tornado was observed on the ground with vorticity exceeding 3 x 10^{-2} s^{-1}. The diameter of the mesocyclone continued to contract toward ~2 km at 1542 while V_{rot} ceased to increase after 1530 with vorticity exceeding 4.5 x 10^{-2} s^{-1}. This could be a sign of the mesocyclone vortex intensifying and collapsing in size into a tornado vortex as documented in Wakimoto et al. (1998). However, the Guangzhou radar's beamwidth (~400 m) was too coarse to resolve the tornado (~200 m wide) at a distance of ~25 km from the radar. It is noted that the lowest elevation of Guangzhou radar was 0.5° where the lowest level of the mesocyclone can be better sampled as it moved closer to the Guangzhou radar from 1436 to 1546. EF3 tornado damages coincided with the time of peak mesocyclone strength. This was consistent with previous studies that ~90% of EF3–EF5 tornadoes were associated with strong mesocyclones (e.g, Smith 1965). The mesocyclone intensity weakened and diameter broadened after 1536 (Fig. 5).

3.2 Tornado vortex signature (TVS)

A tornado vortex signature (TVS), defined as a signature with local maximum and minimum over an azimuthal distance of approximately one beamwidth (< 1 km) and the gate-to-gate azimuthal radial velocity difference (ΔV) greater than 20 m s^{-1} (Brown et al. 1978), was first detected at 1526 at 1.5° elevation (about 1.5 km AGL) near LY (Fig. 4b). In the next 4 min ~1530, the TVS intensified. It strengthened rapidly and descended toward the surface. It could be detected at all elevations below 9.9° except 0.5° (Fig. 5). The lack of consistent TVS at 0.5° can be attributed to the strong second trip echo contaminating the radial velocity data in the TVS region. In fact, the video of funnel cloud taken nearby shows that the tornado was on the ground during this period. The extreme radar reflectivity (> 60 dBZ) in the hook echo at 1536 and 1542 also is suggestive of a tornado debris signature. The first surface damage was identified near LS ~1528. The TVS at all elevations below 3.3° continued to intensify with ΔV greater than 45 m s^{-1}. The strongest TVS was detected at the 0.5° PPI with a magnitude of ΔV~48 m s^{-1} and was collocated with the severe damage exemplified by the fallen trees and demolished factories near location LY. In the next 6 min, the low-level TVS intensity decreased below 30 m s^{-1}. The strongest damage occurred at location MD ~1540 when a cement pole with a diameter of 0.5 m was snapped, supporting an EF3 tornado. After that, the TVS continued to weaken, coincident with the weak damages between locations JB and QK. From 1600 onwards, the TVS became undetectable in radar data, consistent with the end of the damage pattern north of location QK.

4. Kinematic structure of the miniature supercell

Doppler radial velocities from Guangzhou and Shenzhen radars were first interpolated onto a 1 km × 1 km × 1 km Cartesian grid using the National Center for Atmospheric Research's REORDER software (Oye et al. 1995) then synthesized into 3-D winds using CEDRIC (Mohr et al. 1986). The miniature supercell motion (~21.7 m s^{-1} towards an azimuth of 330° relative to true north) was accounted for in the interpolation procedure. Although the Guangzhou radar is closer to the tornado, the scale of the dual-Doppler syntheses is determined by the coarser sampling resolution from the Shenzhen radar ~80 km from the tornado. As a result, the dual-Doppler syntheses can only resolve the parent mesocyclone and the miniature supercell. The evolution and intensification of the mesocyclone circulation at the southeast end of the miniature supercell are illustrated using the storm-relative wind vectors at 1.5 km and 3.5 km altitude (Fig. 6).

The storm-relative velocity field at 1.5 km AGL is dominated by a closed cyclonic circulation (Fig. 6a). The mid-level inflow (Fig. 6b) came from the southwest, and turned cyclonically towards north after it entered the storm. The vorticity maximum is located northeast of the low-level vorticity center, indicating tilting of the low-level horizontal vorticity aligned with the storm motion, consistent with the low-level shear vector as shown in Fig. 3. At 1500 (Fig. 6c-d), the mesocyclone at low levels intensified with its vorticity center collocated with the maximum updraft. The wind fields in the midlevel became more southerly. Thirty minutes later at 1530 (Fig. 6e-f), the magnitude of the mesocyclone, accompanied by a hook echo, intensified by more than 100% with the vorticity maximum exceeding 2×10^{-2} s^{-1} and its diameter decreased to less than 5 km (based on the 5×10^{-3} s^{-1} vorticity contour). The tornado occurred near the center of the cyclonic circulation. Note that the vorticity maximum (i.e., the mesocyclone) is shifted to north of the updraft center. The cyclonic circulation is well defined in the midlevels (Fig. 6f).

Figure 7 presents two orthogonal vertical cross sections of reflectivity, vertical velocity, and vertical vorticity through the mesocyclone center. The miniature supercell and its mesocyclone are seen to extend up to 8 km and 4 km based on the 20 dBZ and 5×10^{-3} s^{-1} contour, respectively, with the maximum vorticity $\sim 2 \times 10^{-2}$ s^{-1} at 2 km AGL. These characteristics are consistent with those miniature supercells observed in TC rainbands in the US (e.g, Spratt et al. 1997; Mccaul et al. 2004; Eastin et al. 2009). The storm-relative inflow approaches from the northeast, and the primary updraft extends from the boundary layer up to ∼6 km with a maximum of ∼10 m s^{-1} at the 3 km altitude. A moderate downdraft with a maximum of ∼6 m s^{-1} is confined to the north of the updraft within the inflow region, which can be attributed to the compensating downdraft of the convective updraft and the drag by heavy precipitation (> 45 dBZ). The tornado is located at the boundary between the updraft and downdraft.

To examine the intensifying mechanism of the mesocyclone in this miniature supercell, the vertical vorticity budget from the 3D dual-Doppler winds is calculated using the method described in Eastin et al. (2009). Ignoring contributions from frictional and solenoidal terms that are usually much smaller, the time rate of change of vertical vorticity can be expressed as the sum of horizontal (HADV) and vertical (VADV) advection of vertical vorticity, the convergence (CONV, or stretching) and tilting (TILT) terms. Figure 8 shows the horizontal distribution of the vertical vorticity production terms at 1.5 km in the vicinity of the mesocyclone at 1500 and 1530, corresponding to the times before and near tornadogenesis, respectively. At 1500 LST (Fig.8a-d), the CONV term is mostly positive within the mesocyclone. The tilting term is comparable in magnitude to the CONV term, and has positive contributions to the vorticity of the mesocyclone. Both HADV and VADV terms exhibit a pair of positive and negative maxima near the center of the mesocyclone, consistent with the effect of advection by the storm-relative winds and vertical motion. Overall, the low-level vorticity production before the tornadogenesis mostly resulted from the tilting of horizontal vorticity and its subsequent stretching.

Near the tornadogenesis time ~1530 (Fig.7e-h), CONV and HADV terms increased to an order of magnitude larger than VADV and TILT terms. The HADV still exhibits a positive (negative) maximum at the southwest (northeast) flank of the mesocyclone center. Maximum CONV exceeds 25×10^{-6} s^{-2} and is collocated with the mesocyclone, indicating its dominant role in the production of vertical mesocyclone vorticity. The vorticity distribution and evolution in this event are consistent with supercells found in the US Great Plains, where the vertical vorticity couplet is initially created by tilting from horizontal environmental vorticity, then positive vorticity is rapidly intensified by the stretching of vertical vorticity within the mesocyclone (e.g, McCaul and Weisman 1996; Davies-Jones et al. 2001).

Past studies (e.g., Markowski et al. 2002; Dawson et al. 2010) have pointed to the importance of cold pool, including its strength in tornadic storms. Often cold pools that are not tool cold or too weak are most favorable for tornado formation. For the miniature supercell storm studied here, the cold pool was rather weak; the surface temperature drops were less than 1 K at surface stations near the path of the tornado (not shown), which is not surprising because of the very humid low-level environment. Because of the weak cold pool, baroclinic generation of horizontal vorticity as a contributor of the low-level vorticity source appears low, while strong vertical shear near the surface associated with surface friction may have played a larger role (Schenkman et al. 2014; Roberts et al. 2016). The relatively low spatial and temporal resolutions of the Doppler wind analyses as well as the lack of data very close to the ground, unfortunately, prevent us from performing detailed trajectory or circulation-based vorticity budget analyses to address the question of the source of tornadic vorticity near the ground. High-resolution simulations studies will be needed to help address such questions.

5. Concluding remarks

The first look of the evolution and structure of a miniature supercell in Typhoon Mujigae (2015), which produced an EF3 tornado, the strongest tornado embedded in a typhoon rainband ever observed in China, was presented in this paper using single and dual-Doppler radar data along with rawinsonde and damage surveys. The tornadic typhoon mini-supercell was embedded in an environment of a moderate CAPE and a strong low-level shear similar to its US hurricane counterparts. Mesocyclone properties deduced from single-Doppler radar data suggest that the mesocyclone first intensified and contracted at ~3 km altitude, then descended to the lower levels. Due to the limitations of the available data, we are unable to investigate the tornadogenesis and the subsequent evolution and structure of the tornado.

With dual-Doppler wind analyses, the parent mesocyclone can be well identified initially. Positive vorticity intensified as the hook echo reflectivity signature developed. The vorticity budget demonstrated that tilting of the low-level horizontal vorticity into the vertical and subsequently stretching by strong updraft were the main contributors to the mesocyclone intensification. Future studies will examine the microphysical processes of the miniature supercell using dual-polarization data from the Hong Kong radar. In addition, storm dynamics and tornadogenesis will be examined using high-resolution numerical simulations that include radar data assimilation.

Acknowledgements

This work was primarily supported by the National Fundamental Research 973 Program of China (2013CB430100), the National Natural Science Foundation of China (grants 41322032, 41275031 and 41230421), and the Social Commonwealth Research Program (GYHY201006007). We would like to acknowledge the China Meteorological Administration for organizing damage surveys and collecting the radar data used in this study. Special thanks also go to all people who took part in the tornado damage survey and shared their valuable pictures and videos of the tornado damage. We would also like to acknowledge Mr. Huang Sheng who shared his valuable videos of the tornado.

Reference

Andra, D. L., 1997: The origin and evolution of the WSR-88D mesocyclone recognition nomogram. *Conference on Radar Meteorology, 28 th, Austin, TX*, 1997.

Brown, R. A., L. R. Lemon, and D. W. Burgess, 1978: Tornado detection by pulsed Doppler radar. *Monthly Weather Review*, **106,** 29-38.

Davies-Jones, R., R. J. Trapp, and H. B. Bluestein, 2001: Tornadoes and tornadic storms. *Severe convective storms*, Springer, 167-221.

Dawson, D. T., II, M. Xue, J. A. Milbrandt, and M. K. Yau, 2010: Comparison of evaporation and cold pool development between single-moment and multi-moment bulk microphysics schemes in idealized simulations of tornadic thunderstorms. *Mon. Wea. Rev.*, **138,** 1152-1171.

Eastin, Matthew D Link, and M. Christopher, 2009: Miniature supercells in an offshore outer rainband of Hurricane Ivan (2004). *Monthly Weather Review*, **137,** 2081-2104.

Edwards, R., 2012: Tropical cyclone tornadoes: A review of knowledge in research and prediction. *E-Journal of Severe Storms Meteorology*, **7**.

Fan, W. and X. Yu, 2015: Characteristics of Spatial-Temporal Distribution of Tornadoes in China. *Meteorological Monthly*.

Glickman, T., 2000: Glossary of meteorology**,** 2nd ed. Amer. Meteor. Soc., 855 pp.[Available online at http://glossary.ametsoc.org.].

Green, B. W., F. Zhang, and P. Markowski, 2011: Multiscale processes leading to supercells in the landfalling outer rainbands of Hurricane Katrina (2005). *Weather and Forecasting*, **26,** 828-847.

Lee, R. R. and A. White, 1998: Improvement of the WSR-88D mesocyclone algorithm. *Weather and forecasting*, **13,** 341-351.

Lee, W. C., M. M. Bell, and K. E. Goodman, 2008: Supercells and mesocyclones in outer rainbands of Hurricane Katrina (2005). *Geophysical Research Letters*, **35**.

Markowski, P. M., J. M. Straka, and E. N. Rasmussen, 2002: Direct surface thermodynamic observations within the rear-flank downdrafts of nontornadic and tornadic supercells. *Mon. Wea. Rev.*, **130,** 1692-1721.

Mccaul, E. W., 1987: Observations of the Hurricane ``Danny'' Tornado Outbreak of 16 August 1985. *Monthly Weather Review*, **115,** 1206.

Mccaul, E. W., 1991: Buoyancy and Shear Characteristics of Hurricane-Tornado Environments. *Monthly Weather Review*, **119,** 1954.

McCaul, E. W. and M. L. Weisman, 1996: Simulations of Shallow Supercell Storms in Landfalling Hurricane Environments. *Mon. Wea. Rev.*, **124,** 408-429.

Mccaul, E. W., D. E. Buechler, S. J. Goodman, and M. Cammarata, 2004: Doppler Radar and Lightning Network Observations of a Severe Outbreak of Tropical Cyclone Tornadoes. *Monthly Weather Review*, **132,** 1747.

McDonald, J. R. and K. C. Mehta, 2006: *A recommendation for an Enhanced Fujita scale (EF-Scale)*. Wind Science and Engineering Center, Texas Tech University.

Meng, z. and d. Yao, 2014: Damage Survey, Radar, and Environment Analyses on the First-Ever Documented Tornado in Beijing during the Heavy Rainfall Event of 21 July 2012. *Weather & Forecasting*, **29,** 702-724.

Mohr, C. G., L. Jay Miller, R. L. Vaughan, and H. W. Frank, 1986: The merger of mesoscale datasets into a common Cartesian format for efficient and systematic analyses. *Journal of Atmospheric and Oceanic Technology*, **3,** 143-161.

Oye, R., C. Mueller, and S. Smith, 1995: Software for radar translation, visualization, editing, and interpolation. *Preprints, 27th Conf. on Radar Meteorology, Vail, CO, Amer. Meteor. Soc*, 359-361.

Roberts, B., M. Xue, A. D. Schenkman, and I. Daniel T. Dawson, 2016: The role of surface friction in tornadogenesis within an idealized supercell simulation. *J. Atmos. Sci.*, **73,** 3371–3395.

Saito, R., M. Fujita, G. Dresselhaus, and M. S. Dresselhaus, 1992: Electronic structure of chiral graphene tubules. *Applied Physics Letters*, **60,** 2204-2206.

Schenkman, A. D., M. Xue, and M. Hu, 2014: Tornadogenesis in a high-resolution simulation of the 8 May 2003 Oklahoma City supercell. *J. Atmos. Sci.*, **71,** 130-154.

Schneider, D. and S. Sharp, 2007: Radar signatures of tropical cyclone tornadoes in central North Carolina. *Weather and forecasting*, **22,** 278-286.

Schultz, L. A. and D. J. Cecil, 2009: Tropical cyclone tornadoes, 1950-2007. *Monthly Weather Review*, **137,** 3471-3484.

Smith, J. S., 1965: The hurricane-tornado. *Mon. Wea. Rev*, **93,** 53-1.

Spratt, S. M., D. W. Sharp, P. Welsh, A. Sandrik, F. Alsheimer, and C. Paxton, 1997: A WSR-88D assessment of tropical cyclone outer rainband tornadoes. *Weather and forecasting*, **12,** 479-501.

Stumpf, G. J., A. Witt, E. D. Mitchell, P. L. Spencer, J. Johnson, M. D. Eilts, K. W.

Thomas, and D. W. Burgess, 1998: The National Severe Storms Laboratory Mesocyclone Detection Algorithm for the WSR-88D*. *Weather and Forecasting*, **13,** 304-326.

Suzuki, H., T. ABE, K. Takaishi, M. Narita, and F. Hamada, 2000: New Polyimides Derived from Norbornanetetracarboxylic Dianhydride and Aromatic Diamine Showing Excellent Transparency and Heat-Resistance. *International Journal of the Society of Materials Engineering for Resources*, **8,** 9-14.

Wakimoto, R. M., C. Liu, and H. Cai, 1998: The Garden City, Kansas, storm during VORTEX 95. Part I: Overview of the storm's life cycle and mesocyclogenesis. *Monthly weather review*, **126,** 372-392.

Xue, M., K. Zhao, M. Wang, Z. Li, and Y. Zheng, 2016: Recent significant tornadoes in China. *Advances in Atmospheric Sciences*, **33,** 1209-1217.

Yu, H., P. Chen, Q. Li, and B. Tang, 2013: Current Capability of Operational Numerical Models in Predicting Tropical Cyclone Intensity in the Western North Pacific. *Weather & Forecasting*, **28,** 353-367.

Zheng, Y., B. Zhang, X. Wang, K. Sun, R. Mu, and W. Xia, 2015: Analysis of typhoon-tornado weather background and radar echo structure. *Meterological Monthly*, **41,** 942-952 (in Chinese with English abstract).

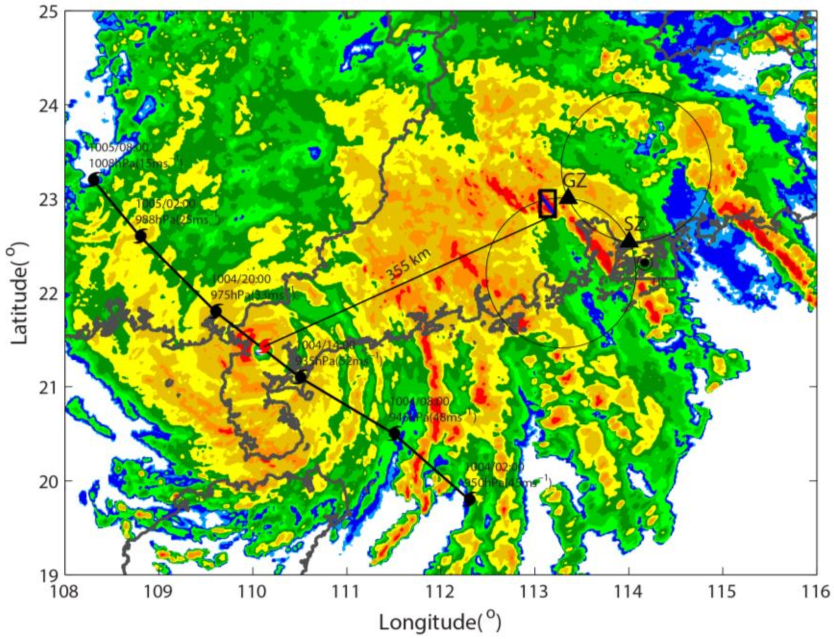

Figure 1. The radar sites (solid triangles) and the sounding station (solid circle) are overlaid on the composite reflectivity of tropical cyclone Mujigae at 1500 LST, October 4, 2015. Two circles show the dual-Doppler radar analysis domain. The TC symbols indicate the TC track, and the black rectangle indicates the region where tornado occurred.

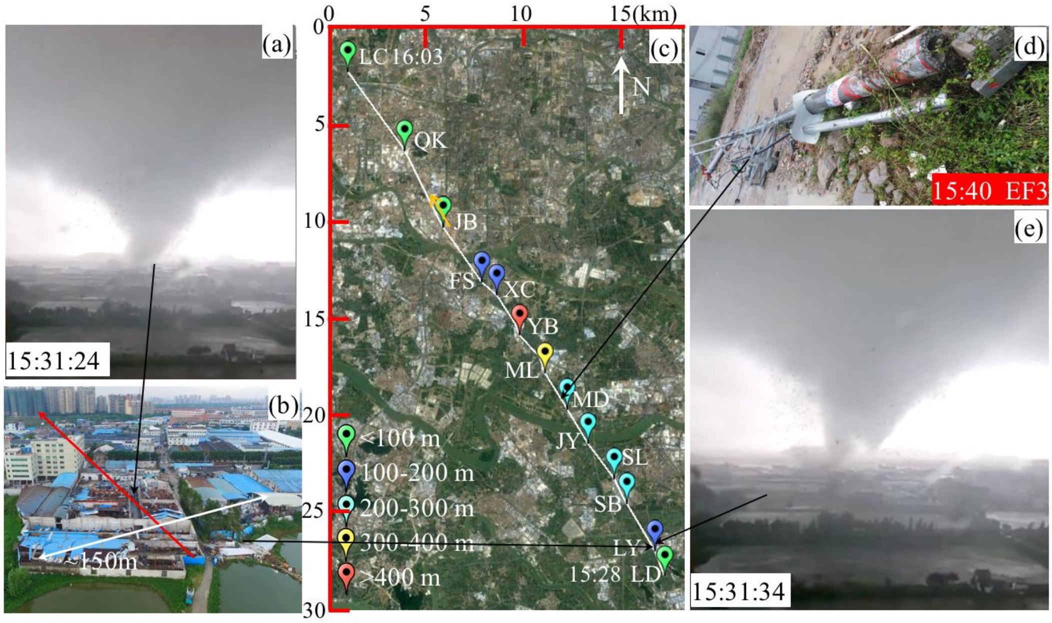

Figure 2. Damage survey of tornado path (middle panel) corresponding to the black rectangle in Fig.1. The visual tornado is viewed from the north and the associated damages are illustrated in the lower left and the upper right panels.

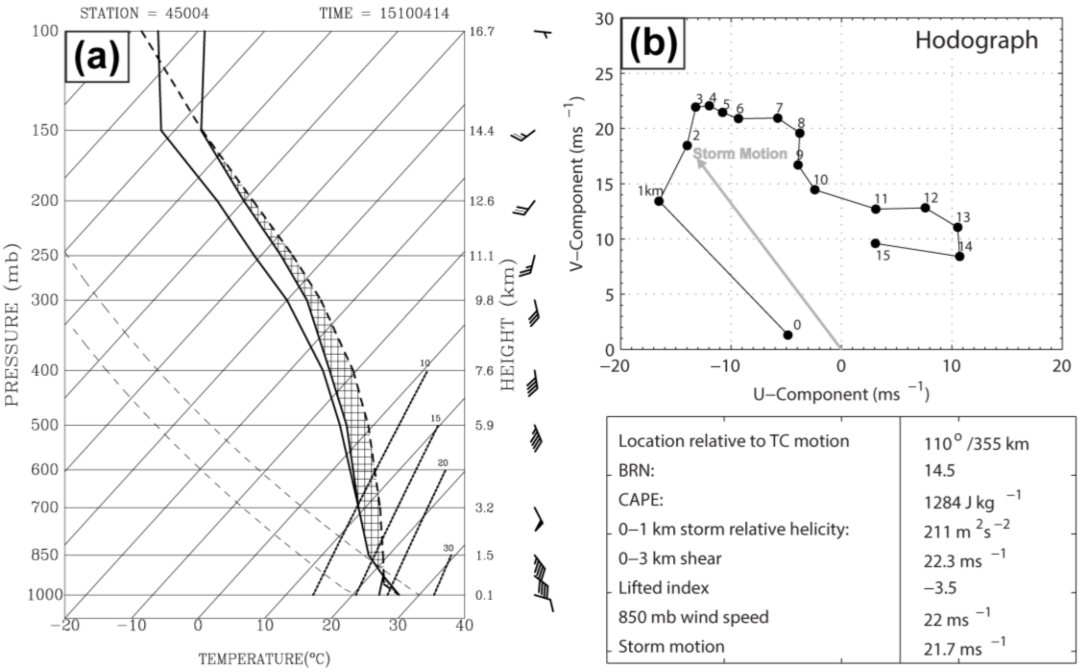

Figure 3. (a) Sounding profile and (b) hodograph at 1400 LST, October 04, 2015, from the Hong Kong Airport. Temperature and dewpoint temperature profiles are represented by solid blue and black lines, while a surface-based parcel path is shown as the red dashed line. The blue area represents the 1284 J Kg^{-1} CAPE for the lifted parcel. Winds (half barb = 5 m s^{-1}; full barb = 10 m s^{-1}) are also shown. The grey arrow in (b) represnts the storm motion.

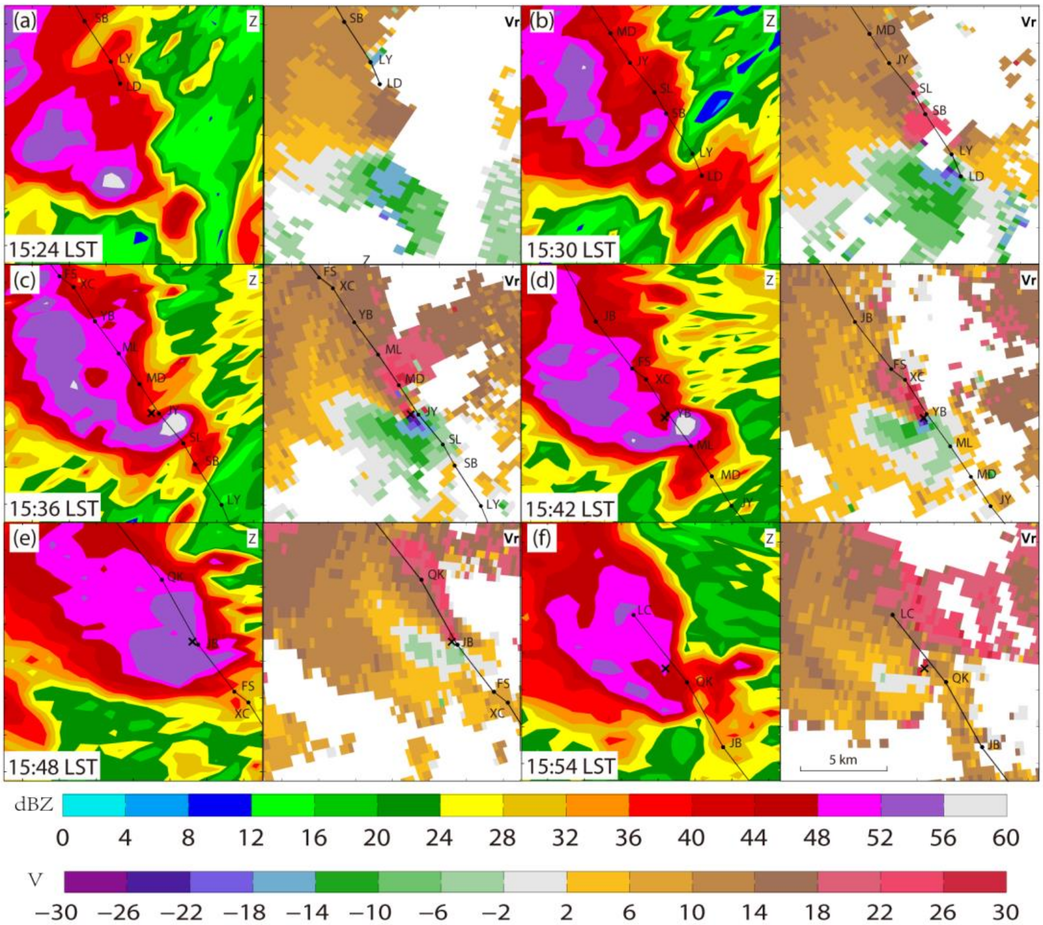

Figure 4. Damage survey of tornado path (solid black line) from Fig. 2 and the TVS (black cross) superimposed on radar reflectivity (dB*Z*) at 1.5° elevation angle from the Guangzhou radar and ground-relative radial velocities (m s^{-1}) from 1524 to 1554 LST, October 4, 2015, at an interval of 6 min.

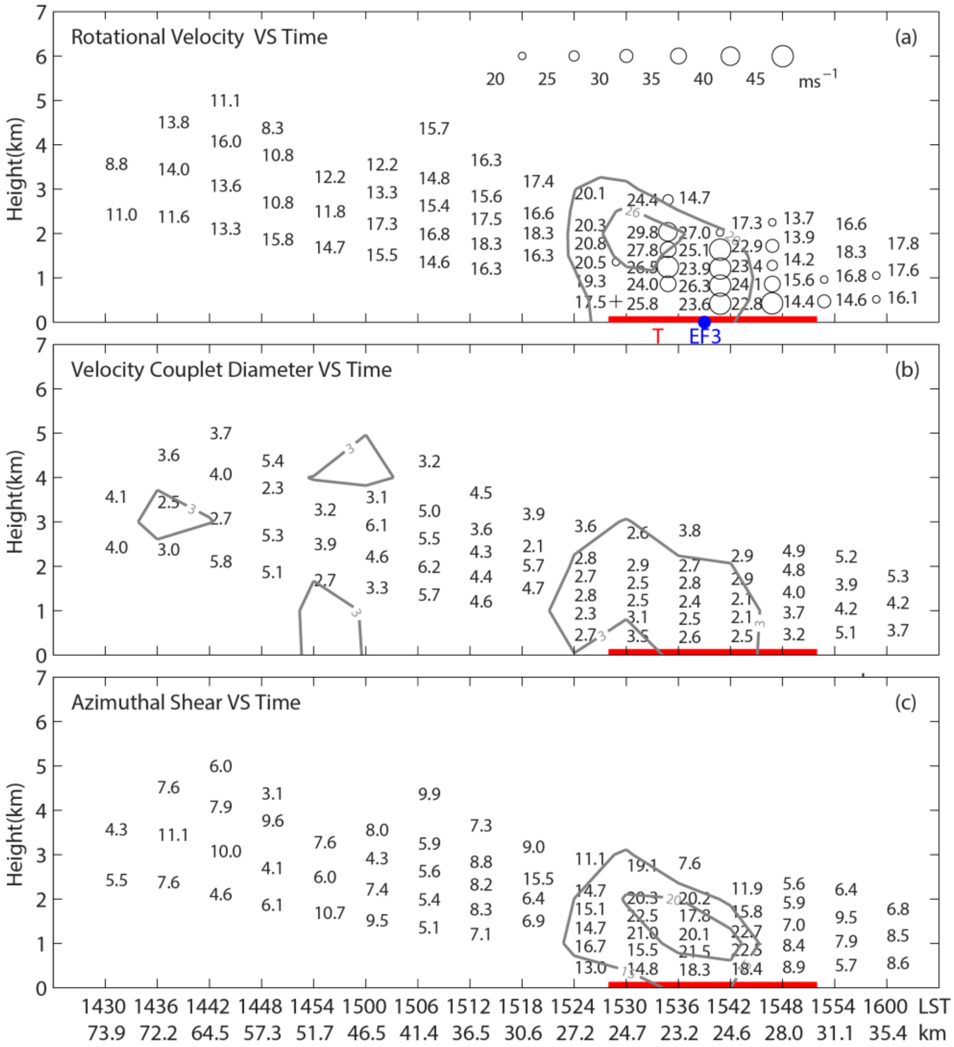

Figure 5. Time-height profiles of (a) rotational velocity (m s^{-1}), (b) couplet diameter (km), and (c) azimuthal shear (10^{-3} s^{-1}) for the tornado's parent mesocyclone. A distance scale (km) relative to Guangzhou radar along with the local time is indicated in the horizontal axis. The strength of the TVS, defined by the gate-by-gate radial velocity difference are indicated by circles in (a). The presence of the tornado, through visual and damage track records, is indicated by the red line.

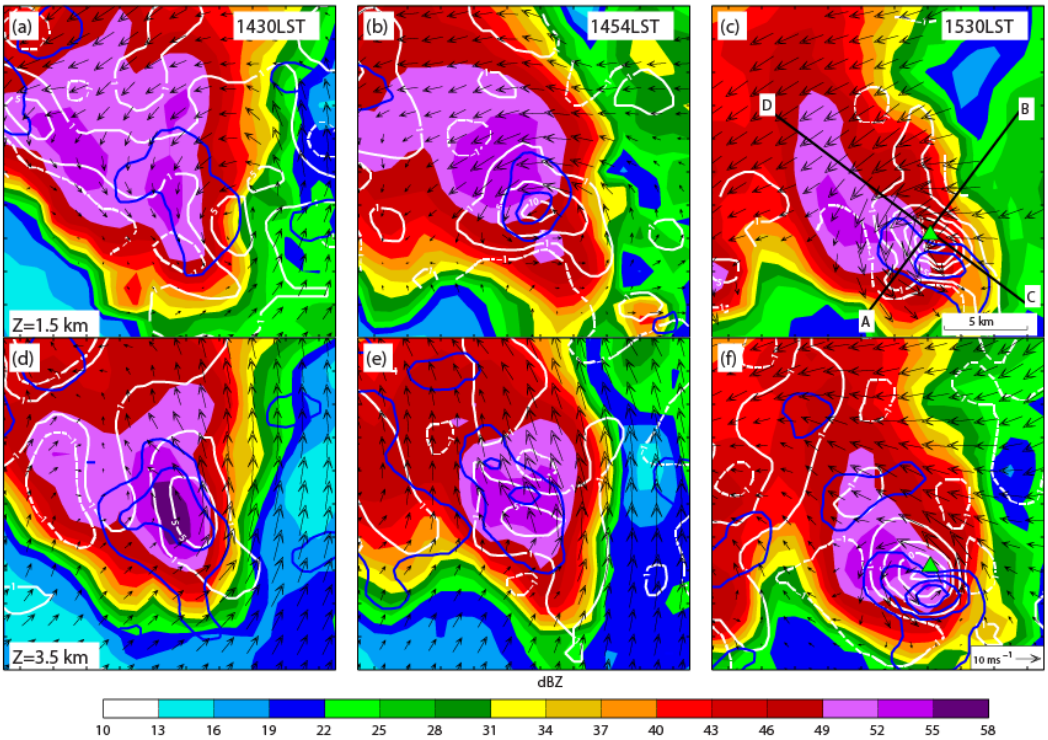

Figure 6. Dual-Doppler analysis of tornadic mesocyclone from Guangzhou and Shenzhen radars at 1.5 km height (top row) and 3.5 km height (bottom row) at (a-d) 1430 LST, (b-e) 1454 LST and (c-f) 1530 UTC, October 04, 2015, corresponds to before and at the time of tornadogenesis. Reflectivity (color, dBZ) is overlaid with storm-relative wind vectors. The positive (white solid line) and negative (white dashed line) vertical vorticity is contoured at ±1, 5, 10, 15, and 20 × 10^{-3} s^{-1}.The updraft (blue line) is contoured at 2, 4, 6, 8,10 m s^{-1}.The green filled triangles indicate the location of the TVS.

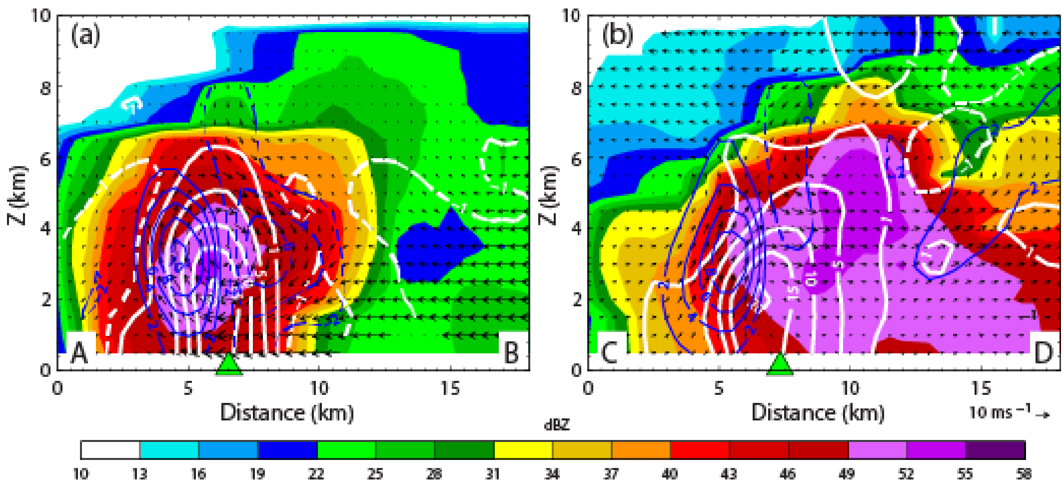

Figure 7. Vertical cross sections of radar reflectivity (dBZ, color shading), storm-relative wind vectors, vertical velocity (m s^{-1}, blue contours), and vertical vorticity (1 ×10^{-3} s^{-1}, white contours) at 1530 LST, October 4, 2015 (at the time of tornadogenesis) along (a) AB and (b) CD in Fig. 5c. The solid and dashed lines denote positive-negative values, respectively. The green filled triangles indicate the location of TVS.

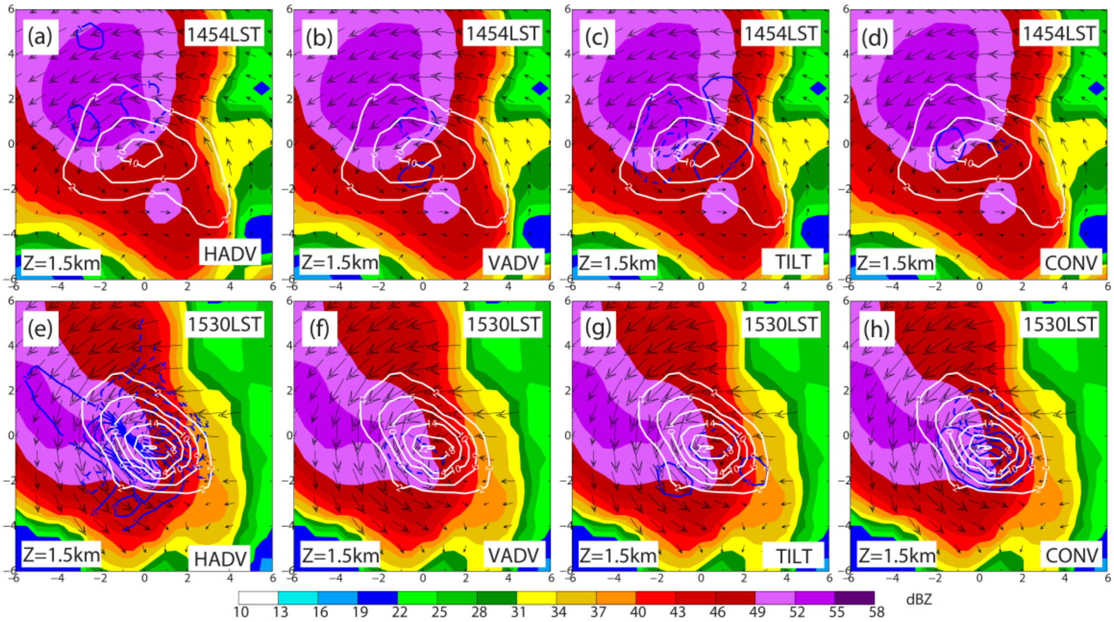

Figure 8. Distributions of (a,e) HADV, (b,f) VADV, (c,g) TILT, and (d, h) CONV terms within the mesocyclone at 1.5 km at 1500 LST (upper row) and 1530 LST (bottom row), corresponding to the times before and near tornadogenesis. Blue solid (dashed) contours denote positive (negative) contributions to vertical vorticity production with the interval of 2×10^{-6} s^{-2}. Reflectivity (dBZ, color shading) is overlaid with storm-relative wind vectors and vertical relative vorticity (white contours with intervals of 4 $\times 10^{-3}$ s^{-1}).